ELSEVIER

Nuclear Instruments and Methods in Physics Research A 453 (2000) 597–605

NUCLEAR INSTRUMENTS & METHODS IN PHYSICS RESEARCH Section A

www.elsevier.nl/locate/nima

An implementation of ionisation energy loss in very thin absorbers for the GEANT4 simulation package

J. Apostolakis[a], S. Giani[a], L. Urban[b], M. Maire[c], A.V. Bagulya[d], V.M. Grichine[d,*]

[a]*CERN, Geneva 23 CH-1211, Switzerland*
[b]*Central Research Institute for Physics, Budapest, Hungary*
[c]*LAPP, BP 110-74941, Annecy-le-vieux, Cedex, France*
[d]*P.N. Lebedev Physical Institute, Lenin Pr. 53, 117924 Moscow, Russia*

Received 21 February 2000; accepted 29 March 2000

Abstract

We discuss an implementation of Photo Absorption Ionisation model describing ionisation energy loss produced by a relativistic charged particle in very thin absorbers. The implementation allows us to calculate ionisation energy losses in any material consisting of elements with atomic numbers in the range 1–100. Comparisons of simulation with the experimental data from gaseous and solid state detectors are presented.

1. Introduction

GEANT4 is an object-oriented toolkit for simulation in High-Energy Physics (HEP), Astrophysics and medical imaging [1]. GEANT4 has exploited advanced software engineering techniques and object-oriented technology to improve the validation of physics results for the simulation of relativistic particle transport through a complex geometry made of different materials and detectors. It is a completely new toolkit, engineered from the start with object-oriented design. In several areas, though, it borrows physical models utilised in GEANT3 simulation package [2]. GEANT4's design divides the responsibilities for different parts of the work into class categories. These include events, geometry, tracking, processes, user interfaces, visualisation and so on [1].

A common structure for modern detectors in HEP consists of a number of thin sensitive gas layers or very thin solid-state (silicon) detectors. In these, the ionisation produced by the penetration of charged particles results in the detector signals. For precise simulation of ionisation energy loss distributions in very thin absorbers, the well-known Landau model is not adequate. Therefore, the most recent Photo-Absorption Ionisation (PAI) model [4,5] was offered in GEANT3 for the simulation of ionisation energy loss in very thin absorbers [2,3]. The implementation of PAI model in GEANT3 was based on an original version of photo-absorption cross-section tables given in Ref. [7] and did not provide adequate description of experimental ionisation energy loss distribution measured in

* Correspondence address: CERN, IT-ADS, Bld513-1-010, CH-1211, Geneva 23, Switzerland. Tel.: +41-22-767-5532; fax: +41-22-767-6555.

E-mail address: vladimir.grichine@cern.ch (V.M. Grichine).

0168-9002/00/$ - see front matter
PII: S0168-9002(00)00457-5

gaseous proportional detectors filled with mixtures of noble and molecular gases.

In the present paper we describe a new implementation of the PAI model for GEANT4, based on the corrected version of photo-absorption cross-section tables. It requires only analytical calculations for the preparation of differential ionisation cross-section. Comparisons with experimental data measured in gaseous and solid state proportional detectors are also presented.

2. Photo-absorption ionization model

Consider the differential cross-section $\mathrm{d}\sigma_i/\mathrm{d}\omega$ of ionising collisions with the energy transfer ω produced by a relativistic charged particle in matter. In its most general form the framework of the PAI model expresses this by the following [5]:

$$\frac{\mathrm{d}\sigma_i}{\mathrm{d}\omega} = \frac{2\pi Ze^4}{\mathrm{mv}^2}\left\{\frac{f(\omega)}{\omega|\varepsilon(\omega)|^2}\left[\ln\frac{2\mathrm{mv}^2}{\omega|1-\beta^2\varepsilon|} - \frac{\varepsilon_1-\beta^2|\varepsilon|^2}{\varepsilon_2}\arg(1-\beta^2\varepsilon^*)\right] + \frac{\tilde{F}(\omega)}{\omega^2}\right\} \quad (1)$$

$$\tilde{F}(\omega) = \int_0^{\omega}\frac{f(\omega')}{|\varepsilon(\omega')|^2}\,\mathrm{d}\omega'$$

$$f(\omega) = \frac{m\omega\varepsilon_2(\omega)}{2\pi^2 ZN\hbar^2}$$

where m and e are the electron mass and charge, respectively, $\hbar$ is the Planck constant, $\beta = v/c$ is the ratio of the particle velocity v to the speed of light c, Z is the effective atomic number, N is the number of atoms (molecule) in unit volume, and $\varepsilon = \varepsilon_1 + \mathrm{i}\varepsilon_2$ is the complex dielectric constant of the medium. In an isotropic non-magnetic medium the dielectric constant can be expressed in terms of complex index of refraction, $n(\omega) = n_1 + \mathrm{i}n_2$, $\varepsilon(\omega) = n^2(\omega)$. In the energy range above the first ionisation potential I_1 for all types of matter of practical interest, and in particular in all gases, $n_1 \sim 1$. Therefore, the imaginary part of the dielectric constant can be expressed in terms of the photo-absorption cross-section $\sigma_\gamma(\omega)$:

$$\varepsilon_2(\omega) = 2n_1n_2 \sim 2n_2 = \frac{N\hbar c}{\omega}\sigma_\gamma(\omega).$$

The real part of the dielectric constant is calculated in turn from the dispersion relation:

$$\varepsilon_1(\omega) - 1 = \frac{2N\hbar c}{\pi}Vp\int_0^{\infty}\frac{\sigma_\gamma(\omega')}{\omega'^2-\omega^2}\,\mathrm{d}\omega'$$

where the integral of the pole expression is considered in terms of the principal value. In practice, it is convenient to calculate the contribution from the continuous part of the spectrum only. Then, we have to use the normalised photo-absorption cross-section $\tilde{\sigma}_\gamma(\omega)$

$$\tilde{\sigma}_\gamma(\omega) = \frac{2\pi^2\hbar e^2Z}{\mathrm{mc}}\sigma_\gamma(\omega)\left[\int_{I_1}^{\omega_{\max}}\sigma_\gamma(\omega')\,\mathrm{d}\omega'\right]^{-1},$$

$\omega_{\max} \sim 100$ keV,

which satisfies the quantum mechanical sum rule [6]

$$\int_{I_1}^{\omega_{\max}}\tilde{\sigma}_\gamma(\omega')\,\mathrm{d}\omega' = \frac{2\pi^2\hbar e^2Z}{\mathrm{mc}}.$$

The differential cross-section of ionising collisions is therefore expressed by the photo-absorption cross-section in the continuous spectrum region

$$\frac{\mathrm{d}\sigma_i}{\mathrm{d}\omega} = \frac{\alpha}{\pi\beta^2}\left\{\frac{\tilde{\sigma}_\gamma(\omega)}{\omega|\varepsilon(\omega)|^2}\left[\ln\frac{2\mathrm{mv}^2}{\omega|1-\beta^2\varepsilon|} - \frac{\varepsilon_1-\beta^2|\varepsilon|^2}{\varepsilon_2}\arg(1-\beta^2\varepsilon^*)\right] + \frac{1}{\omega^2}\int_{I_1}^{\omega}\frac{\tilde{\sigma}_\gamma(\omega')}{|\varepsilon(\omega')|^2}\,\mathrm{d}\omega'\right\} \quad (2)$$

$$\varepsilon_2(\omega) = \frac{N\hbar c}{\omega}\tilde{\sigma}_\gamma(\omega)$$

$$\varepsilon_1(\omega) - 1 = \frac{2N\hbar c}{\pi}Vp\int_{I_1}^{\omega_{\max}}\frac{\tilde{\sigma}_\gamma(\omega')}{\omega'^2-\omega^2}\,\mathrm{d}\omega'.$$

For practical calculations according to Eq. (2) it is convenient to use the representation of the photo-absorption cross-section as a polynomial of ω^{-1} as was proposed in Ref. [7]

$$\sigma_\gamma(\omega) = \sum_{k=1}^{4}a_k^{(i)}\omega^{-k} \quad (3)$$

where the coefficients, $a_k^{(i)}$ are fitted with the experimental data by the least-squares method separately in each ith energy interval. The interval borders are equal, as a rule, to the corresponding photo-absorption edges. Then the dielectric constant can be calculated analytically in elementary functions for all ω, except the photo-absorption edges where the photo-absorption cross section experiences discontinuity and the integral for the real part is not defined in the sense of the principal value.

The third term in Eq. (2), which can be calculated numerically only, results in a complex procedure of calculation of $d\sigma_i/d\omega$. However, calculations show that this term dominates for the energy transfers $\omega > 10$ keV, where the function $|\varepsilon(\omega)|^2 \sim 1$. It is also clear from physical reasons, since the third term represents the Rutherford cross-section on those atomic electrons that can be considered as quasi-free for a given energy transfer [4]. In addition, for high-energy transfers, $\varepsilon(\omega) = 1 - \omega_p^2/\omega^2 \sim 1$, where ω_p is the plasma energy of the matter. Therefore, the factor $|\varepsilon(\omega)|^{-2}$ can be moved from the integral and the differential cross-section of ionising collisions can be expressed as

$$\frac{d\sigma_i}{d\omega} = \frac{\alpha}{\pi\beta^2|\varepsilon(\omega)|^2}\left\{\frac{\tilde{\sigma}_\gamma(\omega)}{\omega}\left[\ln\frac{2mv^2}{\omega|1-\beta^2\varepsilon|} - \frac{\varepsilon_1 - \beta^2|\varepsilon|^2}{\varepsilon_2}\arg(1-\beta^2\varepsilon^*)\right] + \frac{1}{\omega^2}\int_{I_1}^{\omega}\tilde{\sigma}_\gamma(\omega')\,d\omega'\right\}, \quad (4)$$

which is especially simple in gases when $|\varepsilon(\omega)|^{-2} \sim 1$ for all $\omega > I_1$ [4].

3. Photo-absorption cross-section at low energies

The photo-absorption cross-section, $\sigma_\gamma(\omega)$, where ω is the photon energy, is used in GEANT4 for the description of X-ray transportation and ionisation effects in very thin absorbers. For practical calculations it is convenient to use the representation of the photo-absorption cross-section as a polynomial of ω^{-1} as was proposed in Sandia table [7], see Eq. (3). Calculations of primary ionisation and energy loss distributions produced by relativistic charged particles in gaseous detectors based on the original data of Sandia table [8] showed that there is clear disagreement with the experimental data, especially for gas mixtures consisting xenon.

A special investigation was performed in Ref. [8] for the fitting of the coefficients $a_k^{(i)}$ in the energy range of 10–50 eV based on the modern experimental data of synchrotron radiation experiments. The elements usually used in the operation mixture of gaseous detectors were checked. For hydrogen, fluorine, carbon, nitrogen and oxygen the data from the synchrotron radiation experiments with molecular gases such as N_2, O_2, CO_2, CH_4, and CF_4 were used [9,10]. The noble gases were checked using the data given in the tables [11,12].

4. Simulation of energy losses

For a given length of track, the number of ionising collisions is simulated by the Poisson distribution with the mean number proportional to the total cross-section of ionising collisions

$$\sigma_i = \int_{I_1}^{\omega_{max}} \frac{d\sigma_i(\omega')}{d\omega'}\,d\omega',$$

while the energy transfer in each collision is simulated according to the distribution proportional to

$$\sigma_i(>\omega) = \int_{\omega}^{\omega_{max}} \frac{d\sigma_i(\omega')}{d\omega'}\,d\omega'.$$

The sum of the energy transfers in the layer is equal to the energy loss Δ.

Our implementation in GEANT4 involves the following classes for the calculation of the ionisation energy loss in very thin absorbers. The class G4IonisationByLogicalVolume allows to select a material for which the PAI model is applied. By default, for all other materials of the detector simulated, the standard ionisation model (see e.g. Ref. [3]) is used.

At initialisation time the class G4SandiaTable calculates the coefficients $a_k^{(i)}$ for the selected material and perform sorting of the energy intervals. It

uses the photo-absorption cross-section coefficients for elements with atomic number Z in the range 1–100 and their first ionisation potentials I_1 located in the file G4StaticSandiaData.hh. The class G4PAI × Section is responsible for the calculation of the integral ionisation cross-section, the mean number of ionising collisions and the mean ionisation energy loss for the selected material and the given Lorentz factor. The class G4PAIonisation creates the tables of the integral ionisation cross-section, the mean number of ionising collisions and the mean ionisation energy loss for selected material and a set of Lorentz factors are of interest. At the run time of simulation class G4PAIonisation calculates the ionisation energy loss, along the step in the selected material.

5. Comparison with experimental data

5.1. Gaseous proportional detectors

Fig. 1 shows the ionisation energy loss distribution produced by electrons with a momentum of 25 GeV/c in a gas mixture of 80% Ar + 20% CO_2, with a thickness of 1.5 cm (0°C, 1 atm, standard temperature and pressure (STP)). Histogram is the experimental data [13], open circles are simulation according to the PAI model. In this experiment a crosstalk between the adjacent channels of drift chamber was observed. To take into account the crosstalk and shift of zero channel we calculate the energy loss Δ_i according to the following relation recommended in Ref. [13]:

$$\Delta_i = \alpha\Delta_{i-1}^{\mathrm{pai}} + \Delta_i^{\mathrm{pai}} + \alpha\Delta_{i+1}^{\mathrm{pai}} - \beta\bar{S},$$

where $\Delta_{i-1,i,i+1}^{\mathrm{pai}}$ are the energy losses simulated according to the PAI model, $\alpha = -0.055$ is the crosstalk parameter, and $\beta\bar{S} \sim 400 \pm 80$ eV reflects the shift of zero channel. A comparison of the experiment [13] and simulation for the ionisation energy loss distribution produced by protons with a momentum of 25 GeV/c in the same gas mixture is shown in Fig. 2.

Fig. 3 shows the ionisation energy loss distribution produced by protons with a momentum of 3 GeV/c in a gas mixture of 87.5% Xe

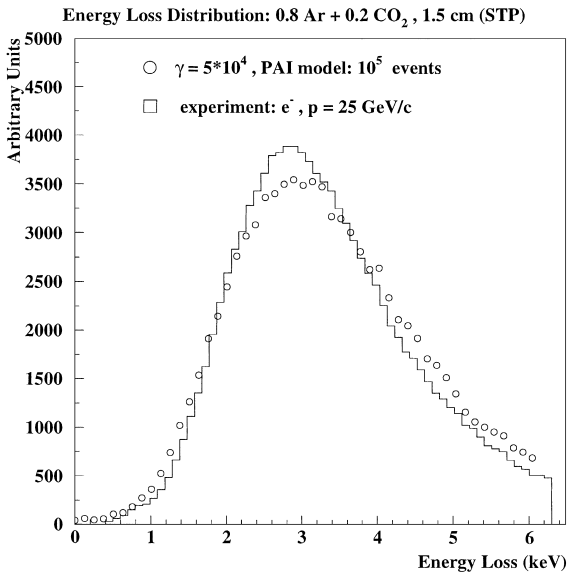

Fig. 1. The ionisation energy loss distribution produced by electrons with a momentum of 25 GeV/c in a gas mixture of 0.8 Ar + 0.2 CO_2 with a thickness of 1.5 cm (STP). Histogram is the experimental data [13], open circles are simulation according to the PAI model.

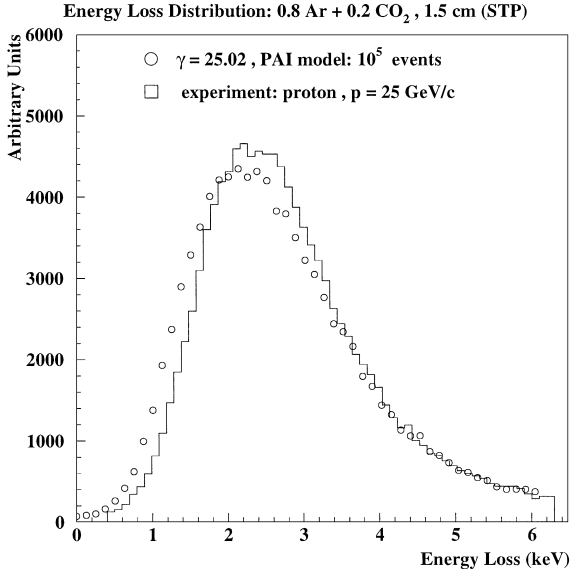

Fig. 2. The ionisation energy loss distribution produced by protons with a momentum of 25 GeV/c in a gas mixture of 0.8 Ar + 0.2 CO_2 with a thickness of 1.5 cm (STP). Histogram is the experimental data [13], open circles are simulation according to the PAI model.

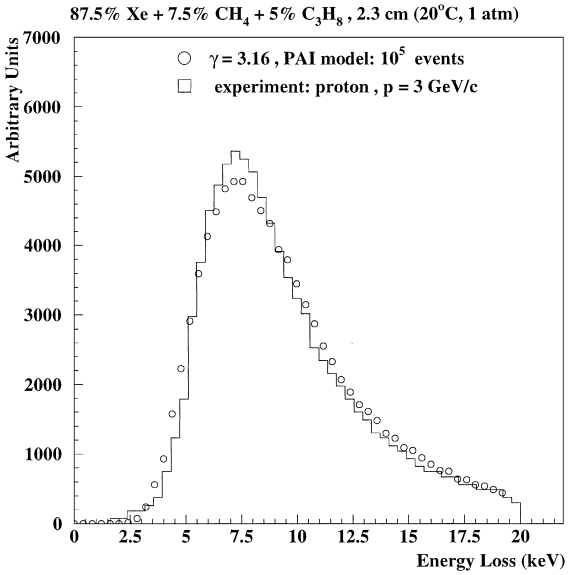

Fig. 3. The ionisation energy loss distribution produced by protons with a momentum of 3 GeV/c in a gas mixture of 87.5% Xe + 7.5% CH_4 + 5% C_3H_8 with a thickness of 2.3 cm (20°C, 1 atm). Histogram is the experimental data [14], open circles are simulation according to the PAI model.

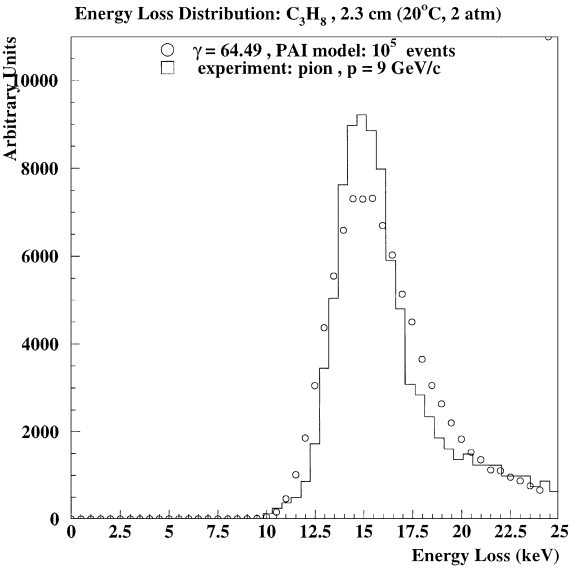

Fig. 4. The ionisation energy loss distribution produced by pions with a momentum of 9 GeV/c in propane with a thickness of 2.3 cm (20°C, 2 atm). Histogram is the experimental data [14], open circles are simulation according to the PAI model.

+ 7.5% CH_4 + 5% C_3H_8 with a thickness of 2.3 cm (20°C, 1 atm). The histogram is the experimental data [14], open circles are simulation according to the PAI model. A comparison of this experiment and simulation for the ionisation energy loss distribution produced by pions with a momentum of 9 GeV/c in propane with a thickness of 2.3 cm (20°C, 2 atm) is shown in Fig. 4.

Fig. 5 shows the ionisation energy loss distribution produced by pions with momentum of 3 GeV/c in a gas mixture of 93% Ar + 7% CH_4 with a thickness of 1.5 cm (STP). The histogram is the experimental data [15], open circles are simulation according to the PAI model. The spike of the last bin corresponds to the number of events with an energy loss more than the upper limit of the histogram. The data shown in Figs. 1–5 were measured in multi-wire gas proportional drift chambers.

Fig. 6 shows the ionisation energy loss distribution produced by electrons with kinetic energy $E_k = 318$ MeV in xenon with a thickness of 8.5 cm (20°C, 1 atm). The histogram is the experimental

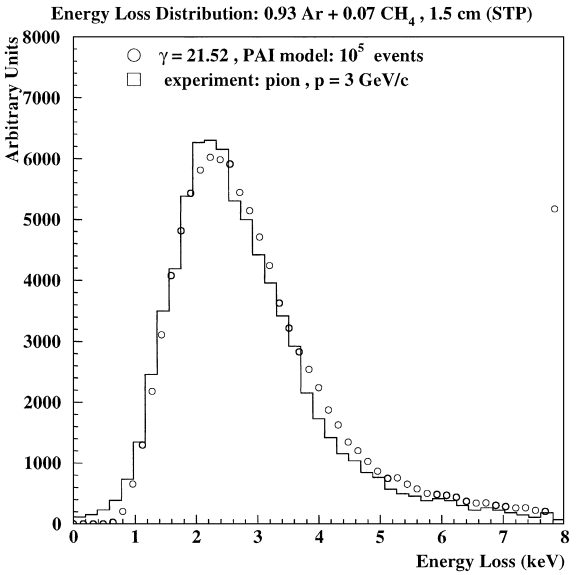

Fig. 5. The ionisation energy loss distribution produced by pions with a momentum of 3 GeV/c in a gas mixture of 93% Ar + 7% CH_4 with a thickness of 1.5 cm (STP). Histogram is experimental data [15], open circles are simulation according to the PAI model.

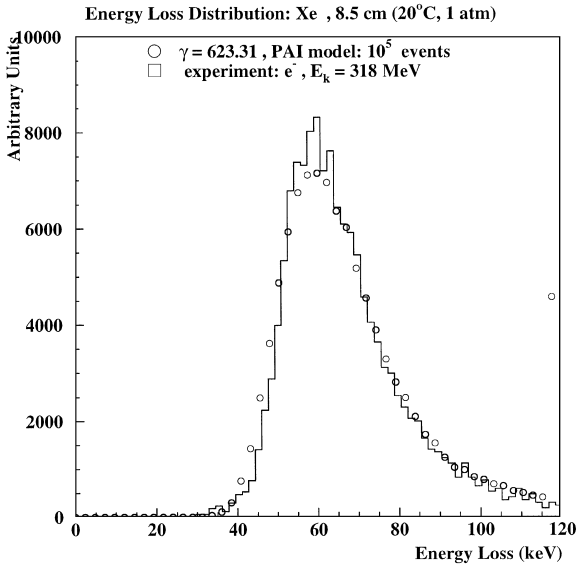

Fig. 6. The ionisation energy loss distribution produced by electrons with the kinetic energy $E_k = 318$ MeV in xenon with a thickness of 8.5 cm (20°C, 1 atm). Histogram is the experimental data [16], open circles are simulation according to the PAI model.

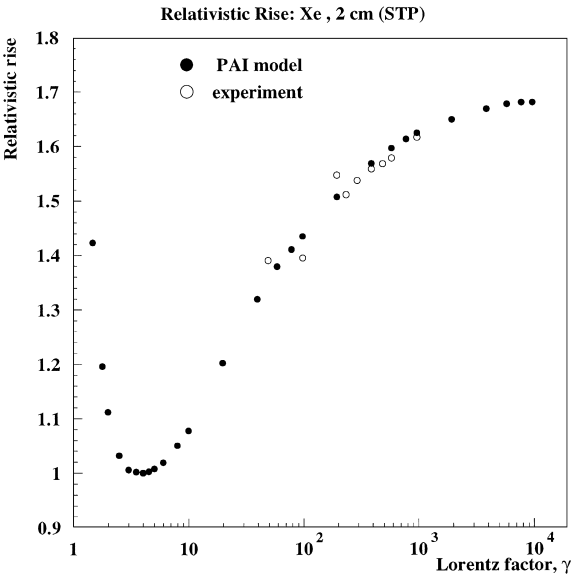

Fig. 7. Relativistic rise of the most probable ionisation energy loss in xenon with a thickness of 2–8.5 cm (20°C, 1 atm). Open circles are the experimental data [16,17], closed circles are simulation according to the PAI model.

data [16], open circles are simulation according to the PAI model. The distribution was measured in gas scintillation proportional drift chamber filled with purified xenon.

In many applications it is interesting to investigate the relativistic dependences of the ionisation energy loss distribution parameters. Fig. 7 shows the relativistic rise $R_r = \Delta_0(\gamma)/\Delta_0(\gamma \sim 4)$ of the most probable ionisation energy loss Δ_0 corresponding to the distribution maximum in xenon with a thickness of 2–8.5 cm (20°C, 1 atm) versus the particle Lorentz factor. Open circles are the experimental data measured in gas scintillation proportional chambers [16,17], closed circles are simulation according to the PAI model. Fig. 8 shows the relativistic rise of the most probable ionisation energy loss in 93% Ar + 7% CH_4 with a thickness of 6 cm (STP) versus the particle's Lorentz factor. Open circles are the experimental data measured in multi-wire drift proportional chamber [18], closed circles are simulation according to the PAI model. One can see from Figs. 1–8 that the simulation according to the PAI model is in good agreement

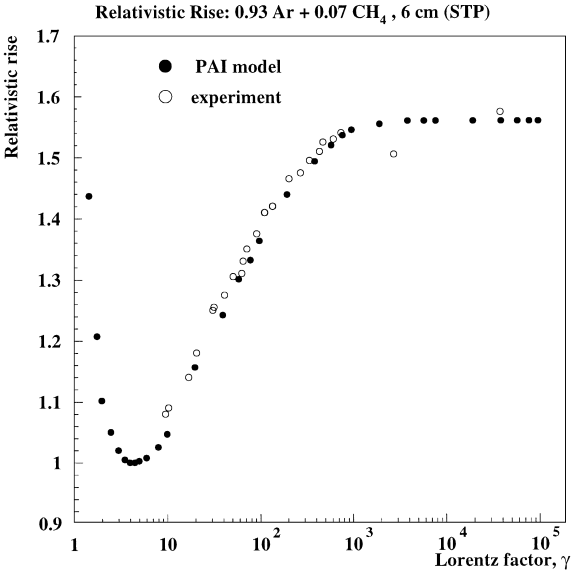

Fig. 8. Relativistic rise of the most probable ionisation energy loss in a gas mixture of 93% Ar + 7% CH_4 with a thickness of 6 cm (STP). Open circles are the experimental data [18], closed circles are simulation according to the PAI model.

with the measurements performed in gaseous proportional detectors.

5.2. Solid state detectors

Fig. 9 shows the ionisation energy loss distribution produced by pions with a momentum of 5 GeV/c in silicon with a thickness of 20.5 μm. Histogram is the experimental data [19,20], open circles are simulation according to the PAI model. In this experiment silicon CCD matrix was used as detector and the ionisation collection distance was estimated to be $\sim$ 16–22 μm, therefore we put the collection distance to be 20.5 μm in accordance with the recommendation of [20]. A comparison of the experiment [21] and simulation for the ionisation energy loss distribution produced by positrons with a momentum of 2 GeV/c in silicon with a thickness of 32 μm is given in Fig. 10. One can observe a small shift between the experimental and simulated distributions since the efficient ionisation collection distance can be a bit smaller than the depletion layer of the detector (32 μm).

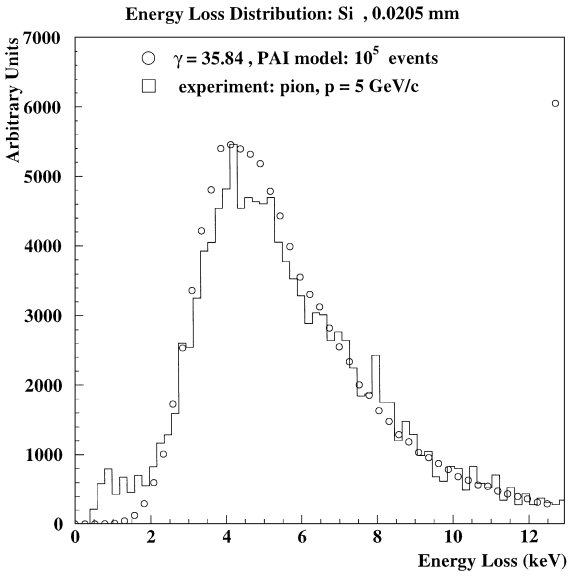

Fig. 9. The ionisation energy loss distribution produced by pions with a momentum of 5 GeV/c in silicon with a thickness of 20.5 μm. Histogram is the experimental data [19,20], open circles are simulation according to the PAI model.

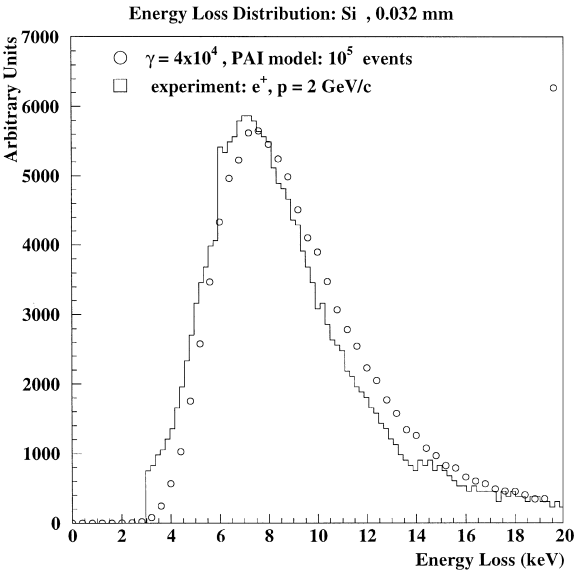

Fig. 10. The ionisation energy loss distribution produced by positrons with a momentum of 2 GeV/c in silicon with a thickness of 32 μm. Histogram is the experimental data [21], open circles are simulation according to the PAI model.

Fig. 11 shows the ionisation energy loss distribution produced by positrons with a momentum of 8 GeV/c in germanium with a thickness of 370 μm. Histogram is the experimental data [21], open circles are simulation according to the PAI model. We observe again a shift between distributions due to overestimation of the efficient ionisation collection distance.

Fig. 12 shows the ionisation energy loss distribution produced by pions with a momentum of 6 GeV/c in GaAs with the collection distance of 85 μm. Histogram is the experimental data [22], open circles are simulation according to the PAI model. The thickness of GaAs diodes was about 125 μm while the best fit shown in Fig. 12 corresponds to a collection distance of 85 μm. Simulation overestimates a bit, the distribution thickness which can be explained by additional recombination of ionisation electrons for collisions with large energy transfers.

Fig. 13 shows the ionisation energy loss distribution produced by electrons with kinetic energy $E_k \sim 1.5$ MeV (^{90}Sr) in polycrystalline diamond

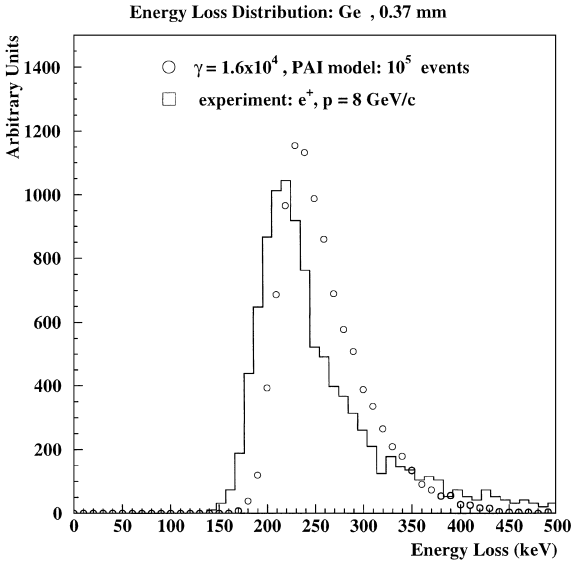

Fig. 11. The ionisation energy loss distribution produced by positrons with a momentum of 8 GeV/c in germanium with a thickness of 370 μm. Histogram is the experimental data [21], open circles are simulation according to the PAI model.

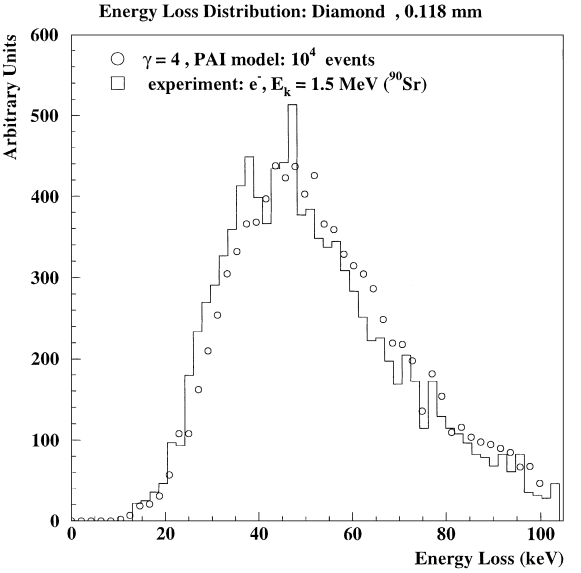

Fig. 13. The ionisation energy loss distribution produced by electrons with the kinetic energy $E_k \sim 1.5$ MeV (^{90}Sr) in polycrystalline diamond with a collection distance of 118 μm. Histogram is the experimental data [23], open circles are simulation according to the PAI model.

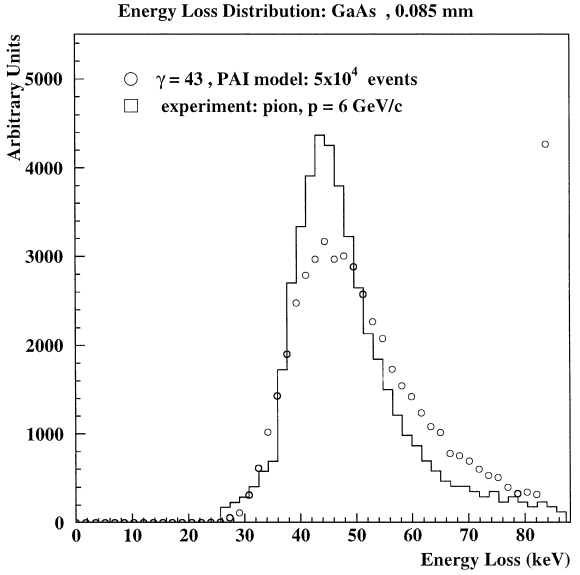

Fig. 12. The ionisation energy loss distribution produced by pions with a momentum of 6 GeV/c in GaAs with a collection distance of 85 μm. Histogram is the experimental data [22], open circles are simulation according to the PAI model.

with a collection distance of 118 μm. The histogram is the experimental data [23], open circles are simulation according to the PAI model. To simulate a broader distribution as compared with direct application of the PAI model, as it is usually observed in diamond detectors, we introduced the additional fluctuations $p(d)$ of the ionisation collection distance d according to the Γ-distribution, as was proposed in Ref. [24]

$$p(d) = \frac{\lambda^a}{\Gamma(a)} d^{a-1} \exp(-\lambda d)$$

$$\langle d \rangle = \frac{a}{\lambda}, \quad D_d = \frac{\langle d \rangle}{\lambda}$$

where $\Gamma(a)$ is the Euler gamma function, a and λ are free positive parameters, $\langle d \rangle$ and D_d are the mean value and variance of d over the Γ-distribution, respectively. The best fit corresponds to $a = 8$ and $\langle d \rangle = 118$ μm.

6. Conclusions

The implementation of the PAI model discussed in the present paper has the following advanced features:

(1) It requires only analytical calculations for the preparation of the ionisation cross-section $d\sigma_i/d\omega$ that accelerates the calculations of tables needed for the simulation of the ionisation energy losses especially for complex detectors with many materials involved.
(2) It is based on the corrected table of the photoabsorption cross-section coefficients $a_k^{(i)}$ for elements usually involved in sensitive material of modern gaseous and solid state detectors.
(3) It allows us to calculate the ionisation energy loss distribution produced by relativistic charged particle in very thin layer of any material consisting of elements with $Z = 1$–100.

A comparison with the experimental data has shown that the simulation of the ionisation energy loss distributions and relativistic dependences of their parameters according to the PAI model is in good agreement with the measurements in gaseous proportional detectors. The agreement of simulation with the experimental data measured in solid state detectors is quite satisfactory. Small shifts observed for Ge and GaAs detectors can be explained by broad distribution of the collection distance of the ionisation electrons. The implementation of the PAI model can be recommended for simulation of the ionisation energy loss distributions produced by relativistic charged particles in very thin absorbers. The code is freely available from the GEANT4 web site [1].

Acknowledgements

We would like to thank Dr. V.A. Chechin and Dr. S.K. Kotelnikov for many fruitful discussions of the points considered in this paper.

References

[1] GEANT4 Collaboration, CERN/LHCC 98-44, GEANT4: An object-oriented toolkit for simulation in HEP; see also the web site: http://wwwinfo.cern.ch/asd/geant4/geant4.html.
[2] GEANT3, CERN Program Library Long Writeup, W5013 (1993).
[3] K. Lassila-Perini, L. Urban, Nucl. Instr. and Meth. A 362 (1995) 416.
[4] W.W.M. Allison, J. Cobb, Annu. Rev. Nucl. Part. Sci. 30 (1980) 253.
[5] V.S. Asoskov, V.A. Chechin, V.M. Grichine et al., Lebedev Inst. Annu. Rep. 140 (1982) 3.
[6] U. Fano, J.W. Cooper, Rev. Mod. Phys. 40 (1968) 441.
[7] F. Biggs, R. Lighthill, Preprint Sandia Laboratory, SAND 87-0070, 1990, 35p.
[8] V.M. Grichine, A.P. Kostin, S.K. Kotelnikov et al., Bull. Lebedev Inst. 2–3 (1994) 34.
[9] L.C. Lee, R.W. Carlson, D.L. Judge et al., J. Quant. Spectrose. Radiat. Transfer 13 (1973) 1023.
[10] L.C. Lee, J. Chem. Phys. 67 (1977) 1237.
[11] G.V. Marr, J.B. West, Atom. Data Nucl. Data Tables 18 (1976) 497.
[12] J.B. West, J. Morton, Atom. Data Nucl. Data Tables 30 (1980) 253.
[13] W.W.M. Allison, C.B. Brooks, J.P. Bunch et al., Nucl. Instr. and Meth. 133 (1976) 325.
[14] A.H. Walenta, J. Fischer, H. Okuno et al., Nucl. Instr. and Meth. 161 (1979) 45.
[15] F. Harris, T. Katsura, S. Parker et al., Nucl. Instr. and Meth. 107 (1973) 413.
[16] W.-D. Herold, J. Egger, H. Kaspar et al., Nucl. Instr. and Meth. 217 (1983) 277.
[17] V.M. Grichine, G.I. Merzon, Nucl. Instr. and Meth. A 274 (1989) 551.
[18] I. Lehraus, R. Mattheson, W. Tejessy et al., Nucl. Instr. and Meth. 153 (1978) 347.
[19] R. Bailey, C.J.S. Damerell, R.L. English et al., Nucl. Instr. and Meth. 213 (1983) 201.
[20] H. Bichsel, Nucl. Instr. and Meth. A 235 (1985) 174.
[21] J.F. Bak, A. Burenkov, J.B.B. Peterson et al., Nucl. Phys. B 288 (1987) 681.
[22] R. Bertin, S. D'Auria, C. Del Para et al., Nucl. Instr. and Meth. A 294 (1990) 211.
[23] F. Hartjes, W. Adam, E. Berdermann et al., Proceedings of Vertex 99, Nucl. Instr. and Meth. A 447 (2000) 244.
[24] V.M. Grichine, A.P. Kostin, S.K. Kotelnikov et al., Nucl. Instr. and Meth. A 352 (1995) 659.